Tricriticality in 4D U(1) lattice gauge theory

Rafael C. Torres,[1,*] Nuno Cardoso,[1,†] Pedro Bicudo,[1,‡] Pedro Ribeiro,[1,2,§] and Paul McClarty[3,4,‖]

[1]*CeFEMA, Instituto Superior Técnico, Universidade de Lisboa, Avenida Rovisco Pais, 1049-001 Lisboa, Portugal*

[2]*Beijing Computational Science Research Center, Beijing 100084, China*

[3]*Laboratoire Léon Brillouin, CEA, CNRS, Université Paris-Saclay, CEA Saclay, 91191 Gif-sur-Yvette, France*

[4]*Max Planck Institute for the Physics of Complex Systems, Nöthnitzer Straße 38, 01187 Dresden, Germany*

(Received 6 June 2024; accepted 27 July 2024; published 30 August 2024)

The 4D compact U(1) gauge theory has a well-established phase transition between a confining and a Coulomb phase. In this paper, we revisit this model using state-of-the-art Monte Carlo simulations on anisotropic lattices. We map out the coupling-temperature phase diagram, and determine the location of the tricritical point, $T/K_0 \simeq 0.19$, below which the first-order transition is observed. We find the critical exponents of the high-temperature second-order transition to be compatible with those of the 3-dimensional $O(2)$ model. Our results at higher temperatures can be compared with literature results and are consistent with them. Surprisingly, below $T/K_0 \simeq 0.05$ we find strong indications of a second tricritical point where the first-order transition becomes continuous. These results suggest an unexpected second-order phase transition extending down to zero temperature, contrary to the prevailing consensus. If confirmed, these findings reopen the question of the detailed characterization of the transition including a suitable field theory description.

DOI: 10.1103/PhysRevD.110.034518

I. INTRODUCTION

Gauge theories formulated on the lattice [1] are central to our understanding of various nonperturbative phenomena such as confinement of color charges in quantum chromodynamics. They are also important in condensed matter physics as emergent low energy theories of interacting spins or electrons in crystalline solids or in quantum simulators. Pure U(1) gauge theory has a long history as a relatively simple example of a theory exhibiting charge confinement at least at strong coupling [2–10]. In three dimensions, Polyakov observed that the theory is confining at all couplings as a consequence of monopole condensation where the existence of monopole charges is a consequence of the compactness of the gauge group [11,12]. In 4D, the analogous excitations can be interpreted as monopole world lines. Polyakov [12] conjectured and Alan Guth proved [13] that there is a phase transition between a strong coupling confined phase and a weak coupling Coulomb phase with propagating photon excitations.

Evidence for this phase transition was found already in Monte Carlo simulations of the lattice action from the 1980s [13–21] and corroborated by later studies [8–10,22–25]. One perspective on this phase transition was as a condensation transition of monopole loops [11,12]. In fact, numerical studies have shown that there is no phase transition if monopole excitations are suppressed [26,27]. An early controversy over the nature of the phase transition at zero temperature was eventually settled in favor of a weak first-order transition [5,9,10,17–25,28–34].

Monte Carlo results are extracted from finite size scaling of simulations performed on lattices of fixed temporal size N_t and spatial extent N_s. Finite temperatures in this theory have been partially explored by simulating lattices with fixed N_t while varying N_s [23–25]. For $N_t = 1$, the 4D U(1) lattice gauge theory (LGT) is decoupled into a 3D U(1) LGT and a 3D XY model. While the 3D U(1) LGT is known to remain in the confining phase throughout the parameter space, the 3D XY model has a second-order phase transition at a finite value of the coupling. As such, one expects a phase boundary connecting the second-order transition at $N_t = 1$ to the first-order transition at $N_t \to \infty$, along which there must be a tricritical point where the order of the phase transition changes. Evidence for this feature of the phase boundary at finite temperature has been seen numerically [25].

*Contact author: rafaelcjtorres@tecnico.ulisboa.pt
†Contact author: nuno.cardoso@tecnico.ulisboa.pt
‡Contact author: bicudo@tecnico.ulisboa.pt
§Contact author: ribeiro.pedro@tecnico.ulisboa.pt
‖Contact author: paul.mcclarty@cea.fr

Further studies considered corrections to the action in the form of the leading higher harmonic of the plaquette term [30,31,35]. These corrections make it possible to shift the position of this tricritical point [30,31]. By tuning the ratio of couplings it is possible to shift the tricritical point to $T = 0$, recovering a second-order transition down to zero temperature [35].

In this paper, we revisit both the nature of the low-temperature transition and the location of tricritical points by providing a unified phase diagram as a function of coupling and temperature for the original Wilson action. It is natural to approach this problem from the perspective of a Hamiltonian formulation of the theory. However, it is the lattice action that can be simulated efficiently using quantum Monte Carlo. Furthermore, the standard lattice action for attainable system sizes provides access only to a very coarse-grained set of temperatures. We provide a systematic Monte Carlo study of the 4D pure U(1) gauge theory addressing both of these issues.

The problem of sweeping in temperature is solved by introducing a continuous anisotropy parameter between the spatial and temporal directions on the lattice. Technically the parallel between the action and the Hamiltonian formulation can be drawn by making use of a Villain approximation at the expense of introducing a renormalization of couplings. To fix this issue, we express all Hamiltonian quantities in terms of the critical coupling at zero temperature. In this way, we are able to systematically relate various anisotropic lattice sizes and couplings of the simulated action to the Hamiltonian couplings and temperature. Using these technical innovations in tandem, we were able to access the finite temperature phase diagram over a wider region of parameter space than hitherto explored. We find direct evidence for a second-order transition at higher temperatures with criticality consistent with the expected 3D XY universality class. As the temperature is lowered and the transition moves to stronger coupling, we pinpoint the location of the tricritical point hinted at in previous studies. At lower temperatures still the first-order transition becomes weaker and in the zero temperature limit our results are compatible both with a continuous and a very weakly first-order transition. Although our results are not precise enough, they suggest a scenario where the zero-temperature transition is continuous concomitant with the existence of an additional tricritical point at low temperature.

The paper is organised as follows. In Sec. II A, we introduce the model and observables, the simulation procedure and lattice anisotropy parameter and the connection to temperature. Then, in Sec. II C, we outline how we identify the phase transition and present the complete finite temperature phase diagram of the 4D U(1) LGT. In Sec. III B, we describe how to determine the order of the transition and present our results revealing a tricritical point. We discuss critical exponents in Sec. III C and summarize all our findings in Sec. IV.

II. U(1) LATTICE GAUGE THEORY

A. Gauge action

We consider a hypercubic lattice with spacetime coordinates labeled as $n = (\tau, r)$, where r labels points on the spatial lattice, and τ the time slice. Directions are labeled as $\mu, \nu = (0, 1, 2, 3)$ with $\mu = 0$ for the temporal direction. The canonical U(1) lattice gauge theory action may be written in terms of angles $\phi_\nu(n) \in [0, 2\pi)$, parametrizing U(1) group elements $U_\nu(n) = e^{i\phi_\nu(n)}$ on links of the lattice. The lattice action is

$$S[\phi] = -\beta \sum_{n,\mu<\nu} \cos \Theta_{\mu\nu}(n), \tag{1}$$

where $\Theta_{\mu\nu}(n) = \phi_\mu(n) + \phi_\nu(n+\hat{\mu}) - \phi_\mu(n+\hat{\nu}) - \phi_\nu(n)$ are terms living on plaquettes. The corresponding quantum theory is defined through the generating function $Z = \int D\phi e^{-S[\phi]}$. The theory has a U(1) gauge invariance under $U_\nu(n) \to \eta(n) U_\nu(n) \eta^\dagger(n+\nu)$ where $\eta(n)$ are local phases.

We define the theory on a lattice with N_s sites along each of the three spatial dimensions, and N_t sites along the temporal direction. Periodic boundary conditions are imposed in all directions.

In the following, it will be convenient to generalize the action in Eq. (9) to anisotropic lattices with different spatial a_s, and temporal, a_t lattice constants. Defining the anisotropy parameter $\xi = a_s/a_t$, spatial and temporal lattice directions have to be treated differently at the level of the action, yielding [36]

$$S[\phi] = -\frac{\beta}{\xi} \sum_{n,l<l'} \cos \Theta_{ll'}(n) - \beta\xi \sum_{n,l} \cos \Theta_{l0}(n), \tag{2}$$

with $l, l' = 1, 2, 3$ denoting the spatial directions.

B. Observables

In a pure U(1) LGT all observables, i.e. gauge-invariant quantities, can be constructed as the trace of the product of link variables across closed loops [37]. Of particular interest for this work is the Polyakov loop at the site r,

$$P(r) = \prod_{j=0}^{N_t-1} U_0(r, j), \tag{3}$$

obtained as the product of temporal link variables along the full extent of the temporal lattice. It corresponds to a closed loop for the considered periodic boundary conditions. The average Polyakov loop,

$$P = \frac{1}{N_s^3} \sum_r P(r), \tag{4}$$

can be interpreted as the probability of observing a single static charge [37] over the probability that no charge is observed.

Therefore, this observable distinguishes confined and deconfined phases. At large values of the coupling constant (small β) we expect the theory to be confined, so that no free charges are observed, i.e. $P = 0$ at the thermodynamic limit. At small values of the coupling constant (large β), we expect the theory to be deconfined, so that free static charges can be observed, i.e. $P \neq 0$. Therefore, the average Polyakov loop can be taken as the order parameter for the confined/deconfined transition. In the following, we use P to determine the critical value β_c at which the phase transition occurs.

For a finite size lattice this translates to the behavior illustrated in the upper panel of Fig. 1. For large values of β we observe $\log\langle P\rangle \propto -N_t$ whereas for small β the asymptotic value reaches an N_t independent constant.

In order to better identify the phase transition, we study the susceptibility of the Polyakov loop, defined as

$$\chi_P = N_t N_s^3(\langle P^2\rangle - \langle P\rangle^2), \tag{5}$$

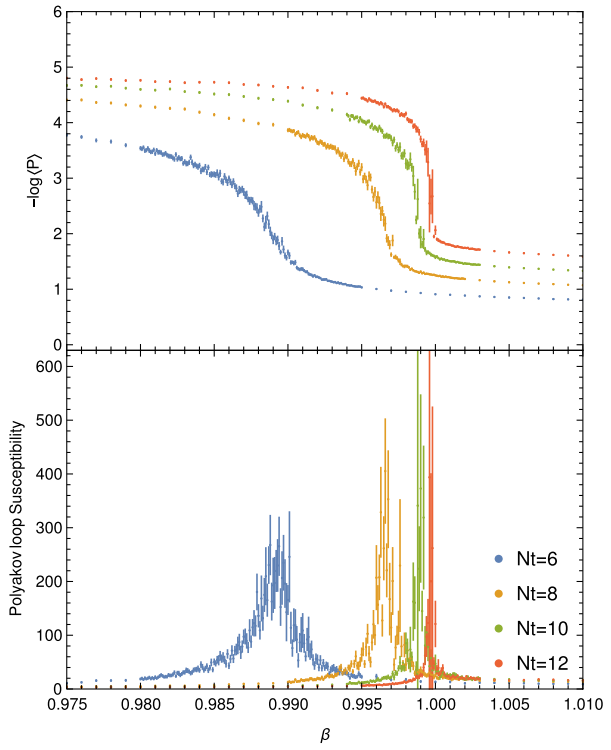

FIG. 1. Logarithm of the average value of the Polyakov loop (top) and Polyakov loop susceptibility (bottom) as a function of β for $N_t = 6$, 8, 10, 12 and $N_s = 24$, for an anisotropic lattice with $\xi = 1.5$. The average Polyakov loop is $P = 0$ in the confining phase, and changes to a nonzero value in the Coulomb phase. The peak in the susceptibility identifies the location of the phase transition.

which peaks at the critical value of β for which the phase transition occurs, as shown in the lower panel of Fig. 1.

C. Simulating the U(1) LGT

To determine the average value of the Polyakov loop and its susceptibility, we carried out Graphics Processing Unit (GPU) accelerated Metropolis-Hastings Monte Carlo [38–43]. We generated $N_{\text{iter}} = 10^5$ Markov Chain iterations and dropped the first 5000, in order to consider only iterations generated after the thermalization of the system. We further calculated the autocorrelation time, τ, between the configurations for several observables, and kept only configurations separated by 3τ. In order to decrease the autocorrelation between two sequential configurations, three over-relaxation steps were implemented [44]. Autocorrelation times for the absolute value of the Polyakov loop between $\tau = 1.4$ and $\tau = 15$ Monte Carlo sweeps were obtained in different regions of the parameter space, resulting in a final number of configurations between $N_{\text{config}} = 22.6 \times 10^4$ and $N_{\text{config}} = 2.1 \times 10^3$. The variance of the observables was calculated with the Jackknife method [45,46].

From these simulations taken for different values of N_t and ξ, we obtain the critical value of $\beta(N_t, \xi)$ for which the confinement/deconfinement phase transition occurs by performing a Lorentzian fit to the Polyakov loop susceptibility. We have checked that results do not change significantly with N_s for N_s sufficiently large.

D. Effective Hamiltonian

To link the coupling constants of the lattice gauge theory defined in the previous section to physical parameters we shall assume that there is a Hamiltonian for the gauge theory with couplings U and K that are to be determined from the lattice action results [47],

$$H = \frac{U}{2}\sum_{r,l}(n_l(r))^2 - K\sum_{r,l<l'}\cos\left[\Theta_{ll'}(r)\right], \tag{6}$$

where $n_l(r)$ an integer-valued operator conjugated to $\phi_l(r)$.

E. Parameter matching

Starting from the Hamiltonian of Eq. (6), the standard derivation of the partition function $Z = \mathrm{Tr}[e^{-H/T}]$ by Trotter slicing, that we sketch in Appendix A for completeness, relies on the Villain approximation to integrate the conjugated variables, $n_\mu(r)$. A naive identification of the resulting action, valid for large values of TN_t/U, and that of Eq. (2) yields

$$\frac{K}{TN_t} = \frac{\beta}{\xi}, \tag{7}$$

$$\frac{TN_t}{U} = \beta\xi. \tag{8}$$

However, at small N_t, there are important corrections at low temperatures. A first refinement to Eqs. (7) and (8) can be obtained using a perturbative expansion [48], which we provide in Appendix B. As we show in Appendix B, despite clear improvements over the naive parametrization Eqs. (7) and (8), this approach is still not sufficient to determine the phase diagram given the system sizes available to us.

Nevertheless, an action of the form of Eq. (2) is expected to capture the physics of H, especially in the vicinity of the phase transition where irrelevant terms can be neglected.

With this motivation, we renormalize the parameters in the action, replacing the coefficient multiplying the space-time part with a scaling function of TN_t/U to be determined, i.e.,

$$S[\phi] = -\frac{K}{TN_t}\sum_{n,\mu<\nu}\cos\Theta_{\mu\nu} - f\left(\frac{TN_t}{U}\right)\sum_{n,\mu}\cos\Theta_{\mu 0}. \tag{9}$$

Identifying the terms with those in Eq. (2) and solving in order to K/U and T/U we find

$$\frac{K}{U} = \frac{\beta}{\xi} f^{-1}(\beta\xi), \tag{10}$$

$$\frac{T}{U} = \frac{1}{N_t} f^{-1}(\beta\xi). \tag{11}$$

To determine $f(z)$ numerically we first approximate the quantity $\beta_0(\xi) = \lim_{N_t\to\infty}\beta(N_t,\xi)$ by $\beta(N_t,\xi)$ computed with the largest available value of N_t and confirm that appropriate convergence with N_t was achieved.

The critical value of $K = K_0$ at $T = 0$ is thus given by Eq. (10) evaluated at $\beta_0(\xi)$

$$\frac{K_0}{U} = \frac{\beta_0(\xi)}{\xi} f^{-1}[\beta_0(\xi)\xi]. \tag{12}$$

Since the left-hand side of this equality is independent of ξ and since $\beta_0(\xi)$ was obtained previously, this relation can be used to determine $f^{-1}(z)$ up to a multiplicative constant, i.e. function $\tilde{f}^{-1}(z) = Uf^{-1}(z)/K_0$. The quantities $\beta_0(\xi)$ and $\tilde{f}^{-1}(z)$ are shown in Figs. 2 and 3, respectively.

Given $\tilde{f}$, the mapping between the action and the Hamiltonian is completely determined by

$$\frac{K}{K_0} = \frac{\beta}{\xi}\tilde{f}^{-1}(\beta\xi), \tag{13}$$

$$\frac{T}{K_0} = \frac{1}{N_t}\tilde{f}^{-1}(\beta\xi). \tag{14}$$

A drawback of this procedure is that it only determines the mapping between Hamiltonian and action coupling constant up to a constant, K_0, that has to be determined independently.

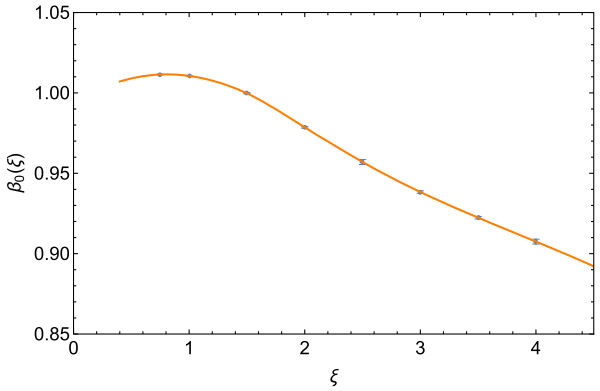

FIG. 2. Values of $\beta_0(\xi) = \lim_{N_t\to\infty}\beta(N_t,\xi)$ for each value of ξ approximated using the largest value of N_t available.

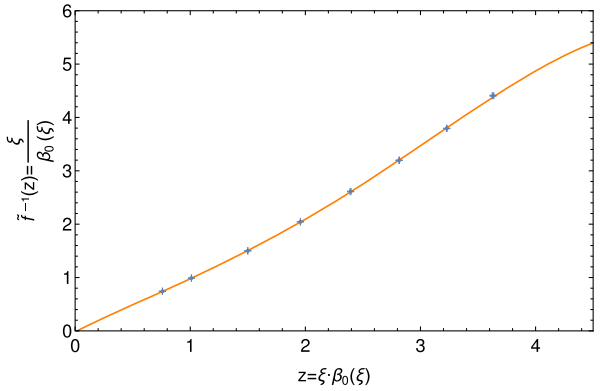

FIG. 3. Function $\tilde{f}^{-1}(z)$ obtained by fitting a curve to $z = \xi\beta_0(\xi)$ and $\tilde{f}^{-1} = \xi/\beta_0(\xi)$, according to Eq. (12) and using the values of β_0 determined for each value of ξ, as shown in Fig. 2.

III. RESULTS

A. Phase diagram

Figure 4 shows the phase diagram of the U(1) gauge Hamiltonian (6), obtained via the approach outlined in the previous section. Using our parameter matching procedure, the critical values of $\beta(N_t,\xi)$, obtained by simulating the lattice action for many different (N_t,ξ) couplings, collapse into a single curve.

The quality of the data collapse is remarkable. As expected, we find that for large T the transition is second order and passes to first order at a tricritical point, TP, as T decreases. Interestingly, for even lower temperature, we find that the discontinuity becomes weaker. In fact, our data are compatible with a second-order transition for $T = 0$. These findings are substantiated in the next section.

B. Order of the phase transition

We now turn to the discussion of the order of the phase transition along the entire phase boundary. To identify the order of the transition, we examine the histograms of the

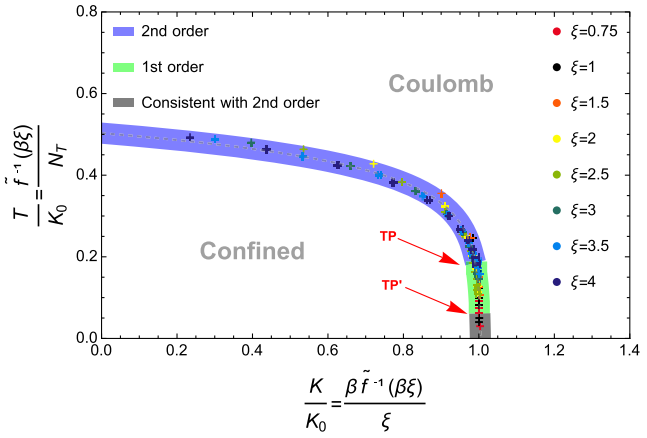

FIG. 4. Phase diagram using the parameters in Eqs. (13) and (14). Different markers represent different extents of the temporal lattice, N_t. The error bars were computed and are smaller than the markers. The calculated values of T/K_0 and K/K_0 for each value of ξ and N_t are presented in Appendix C, in Table I. TP indicates the tricritical point at which the transition changes between first and second order. TP' instead refers to the point below which the transition is consistent with second order.

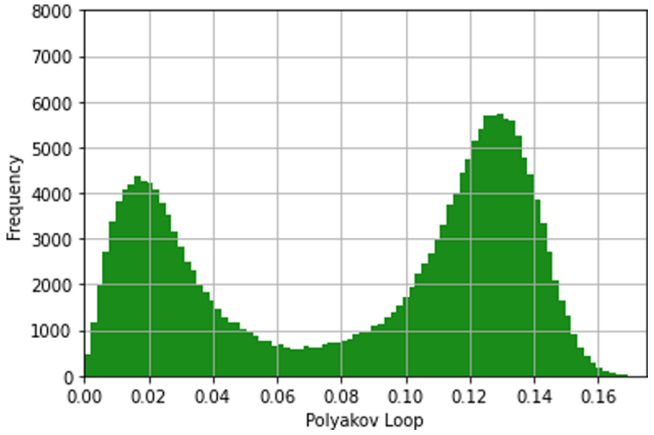

FIG. 5. Histogram of the Polyakov loop at the phase transition for $T/K_0 = 0.12$. The two peaks identify phase coexistence at a first-order transition.

absolute value of the Polyakov loop on both sides of the transition. The first-order nature of the transition is determined from phase coexistence signaled by a double peak structure in the histogram [49].

Histograms are obtained using the field configurations of $N_{\text{iter}} = 200000$ consecutive Markov Chain iterations and discarding the first 5000 in order to remove the pretherm-alization regime. Simulations were carried out with spatial extents $N_s = 24$, and $N_s = 36$.

Figure 5 illustrates the two-peak structure clearly observed at the phase transition for $T/K_0 = 0.12$. Figure 6 shows how the Polyakov loop histogram evolves across the phase transition from the confined to the deconfined phases, for fixed T/K_0 and various K/K_0.

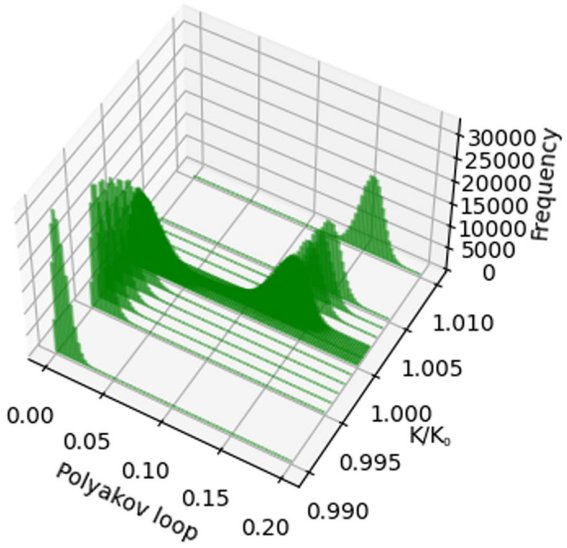

FIG. 6. Histograms of the Polyakov loop for $T/K_0 = 0.12$ and varying K/K_0. Close to the phase transition, we can identify two peaks in the histogram.

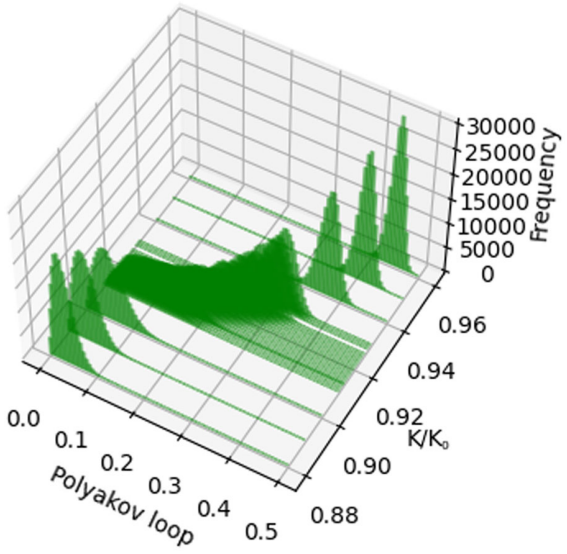

FIG. 7. Histograms of the Polyakov loop at $T/K_0 = 0.32$ and varying K/K_0.

In the confined phase the histogram is single peaked. The two-peak structure appears around the phase transition and vanishes again deeper inside the deconfined phase.

We identify a two-peak structure for temperatures $0.05 < T/K_0 \leq 0.175$ consistent with a discontinuous change of the Polyakov loop as the system transitions from the confined to the Coulomb phase. Accordingly we label transitions in this region as first order.

Figure 7 shows the evolution of the histogram across the phase transition for a temperature $T/K_0 \geq 0.19$. Here, only one peak can be identified in the histogram that is progressively centered at higher values of the Polyakov

loop. This continuous change of the average values of the Polyakov loop is compatible with a second-order phase transition.

From the analysis of the histogram across the transition, our data is consistent with the existence of a temperature point between $T/K_0 = 0.175$ and $T/K_0 = 0.19$ at which the transition changes from first to second order. This high-temperature change in the order of the phase transition had already been explored using isotropic lattices as we now briefly summarize.

In [23], the authors analyzed time histories of the plaquette mean values and found signs of metastability on isotropic lattices with $N_t = 6$ and $N_t = 8$, indicating that the transition is of first order for lattices with these extents in the temporal direction. For a smaller lattice (higher temperature) their results seem to indicate that the transition could be second order for $N_t = 4$. More recently, in [25], the authors conclude that the transition is first order for lattices with $N_t \geq 6$ and second order for lattices with $N_t \leq 5$ by studying the scaling of the plaquette and Polyakov loop susceptibilities with N_s, using isotropic lattices with fixed values of N_t.

The results we report above are in accordance with these previous studies. Moreover, by considering the anisotropic lattice regularization, we are able to explore a wider parameter region, and obtain a comprehensive coupling-temperature phase diagram that reveals the tricritical point connecting the highest temperature regime ($T/K_0 > T_{\mathrm{TP}}$) to intermediate temperatures ($0.05 < T/K_0 < T_{\mathrm{TP}}$). Our numerical analysis of the double-peak structure places the tricritical temperature, T_{TP}, within the interval $0.175 < T_{\mathrm{TP}} < 0.19$. In addition, our method is also able to access the previously unexplored lower temperature regime that we discuss below.

Figure 8 shows the position of the peaks in the Polyakov loop histogram versus temperature for various values of T/K_0. The distance between peaks is plotted in Fig. 9. As expected, from moderate to high temperatures, the peak-to-peak distance vanishes (up to error bars) concomitantly with transition change from first to second order. Surprisingly, for low temperatures, the distance between the peaks also vanishes as the temperature decreases. Indeed, for $T/K_0 \leq 0.05$, the peak-to-peak distances vanish within error bars. Although it is impossible to exclude a very weak first-order transition, these results strongly indicate the existence of a low-temperature tricritical point, TP′, where the transition apparently becomes second order from $T_{\mathrm{TP}'}/K_0 \simeq 0.05$ down to $T = 0$.

As previously mentioned, there has been some debate about the order of the phase transition of the U(1) LGT in the zero temperature limit. This question has been addressed using isotropic lattices [6,10,19,21,22] with an apparent consensus that the transition is first order in the limit of zero temperature. However, isotropic lattice regularization is constrained to specific values of temperature, whereas anisotropic lattices allow one to explore a much wider range of temperatures. In particular, the lattice sizes used in these previous studies [6,10,19,21,22] correspond to temperatures greater than $T/K_0 = 0.05$, for which our method also predicts a first-order transition. It is only for values of the temperature below those considered in previous studies that we find the possibility that the two peaks in the Polyakov loop histogram merge implying a continuous transition below TP′ and down to zero temperature.

In Fig. 4, we present the complete phase diagram with the order of the transition indicated.

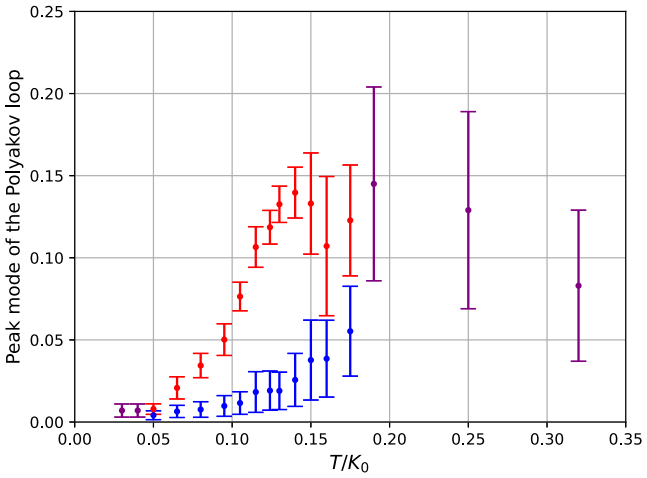

FIG. 8. Position of the peaks in the Polyakov loop histogram for the values of T/K_0 considered. For the cases where two peaks were identified, both peak positions are plotted in blue and red. For the cases where only one peak was identified, the position of the peak at the phase transition is plotted in purple.

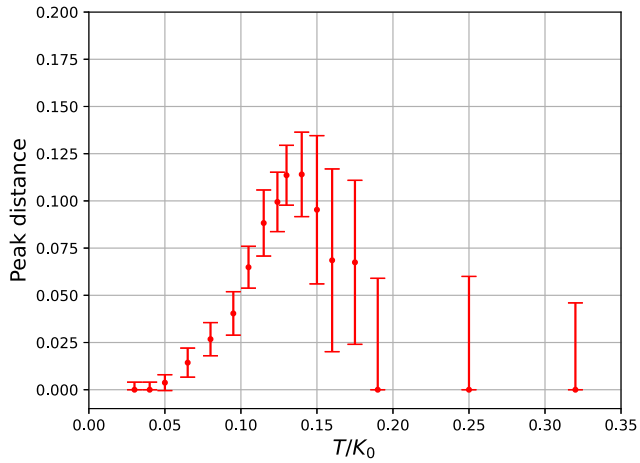

FIG. 9. Distance between the peaks in the Polyakov loop histogram. In the cases where only one peak was identified, the peak distance is plotted at zero and the error bars correspond to the error in the peak position.

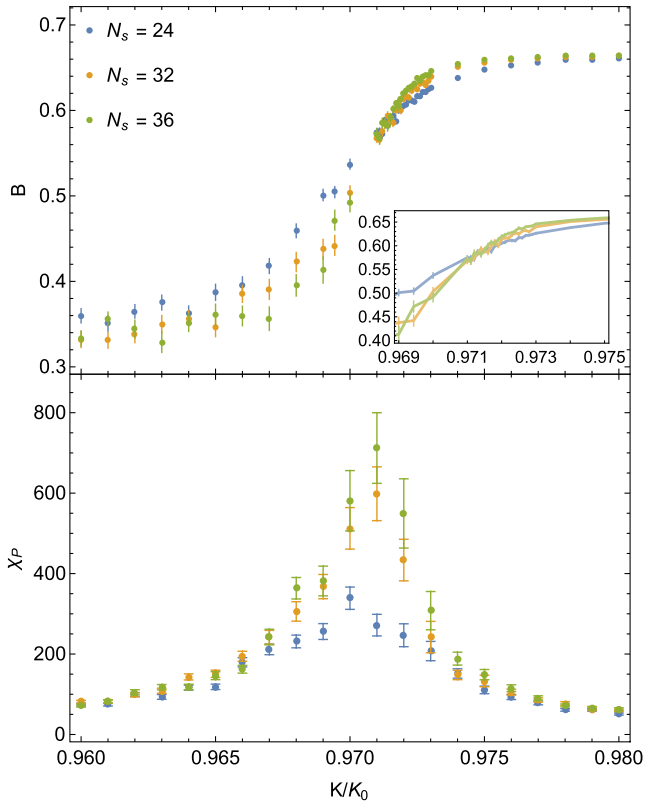

FIG. 10. Binder cumulant (top) and Polyakov loop susceptibility (bottom) at $T/K_0 = 0.25$ and varying K/K_0, for $N_t = 8$ and several values of N_s. The curves of the Binder cumulant for different N_s cross at $(K/K_0)_{\text{crit}} = 0.9715 \pm 0.0005$, indicating the critical value of K/K_0 at infinite spatial volume.

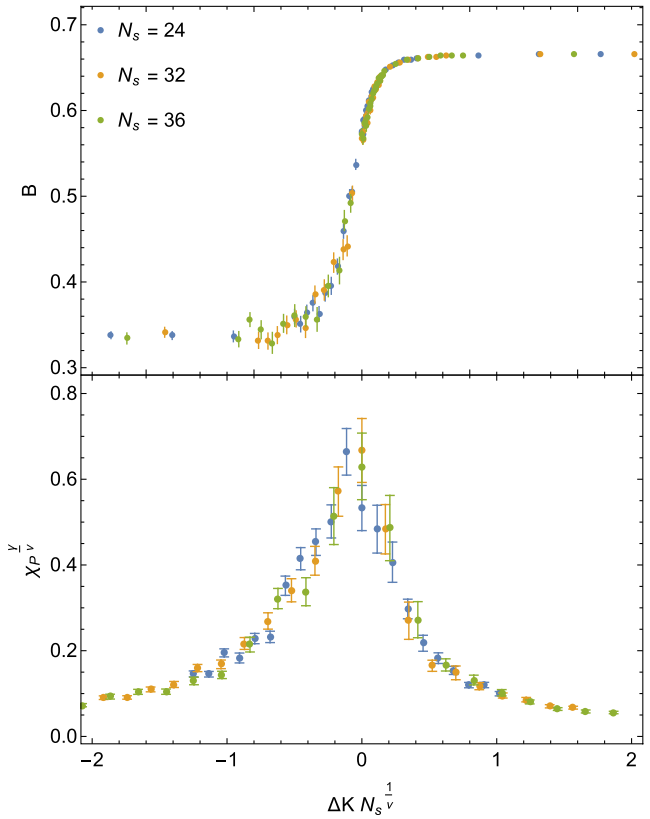

FIG. 11. Data collapse of the Binder cumulant (top) and the Polyakov loop susceptibility (bottom) at $T/K_0 = 0.25$ for different spatial sizes obtained for $\nu = 0.67171$ and with $(K/K_0)_{\text{crit}} = 0.9715$.

C. Critical exponents

In order to examine the nature of the phase transition in the regions $T/K_0 \geq 0.19$ and $T/K_0 \leq 0.05$, we investigated the critical exponents for points in each of these regions.

We calculated the Binder cumulant,

$$B = 1 - \frac{\langle P^4 \rangle}{3\langle P^2 \rangle^2} \tag{15}$$

and the Polyakov loop susceptibility, χ_P, for fixed values of T/K_0 and varying K/K_0, for several values of the spatial volume, while keeping the temporal size, N_t, fixed. Near the phase transition, these quantities scale as

$$\begin{aligned} \chi_P &\sim N_s^{\frac{\gamma}{\nu}} f\left(\Delta K \cdot N_s^{\frac{1}{\nu}}\right) \\ B &\sim f\left(\Delta K \cdot N_s^{\frac{1}{\nu}}\right), \end{aligned} \tag{16}$$

where $\Delta K = (K - K|_{\text{crit}})/K_0$, with $(K/K_0)_{\text{crit}}$ the critical value of K/K_0 at infinite spatial volume, and γ and ν are the critical exponents.

Figure 10 shows the Polyakov loop susceptibility and the Binder cumulant obtained at $T/K_0 = 0.25$. We estimated the critical value $(K/K_0)_{\text{crit}}$ from the crossing of B for different system sizes. Figure 11 depicts the same data scaled with the critical exponents for the 3D XY universality class, $\nu = 0.67171$ and $\gamma = 0.13178$ [25]. The data collapse indicates that the high temperature phase transition of the U(1) lattice gauge theory is of the 3D XY universality class as one would expect as the model maps to the 3D XY model in the $K/K_0 = 0$ limit.

Motivated by the fact that the peak distance in the Polyakov loop histogram goes to zero, we examine the Binder cumulant in order to address the possibility of a second-order transition at low temperatures ($T/K_0 < 0.05$). The transition is harder to probe at low temperatures as the onset of the Binder cumulant is more shallow. Figure 12 shows the Binder cumulant as a function of ΔK for several temperatures. The inset shows that the discontinuity in the Binder cumulant, ΔB, decreases with decreasing temperature. Below, we studied $T/K_0 = 0.03$ where the discontinuity in the Binder cumulant is negligible and where the histogram reveals a single peak. Taking large values of the spatial lattice extent ($N_s = 40$, 46, 50), and with $N_{\text{iter}} = 1.6 \times 10^7$ we obtain Fig. 13 that shows the Binder cumulant varying smoothly across the phase transition which is consistent with a second-order phase transition.

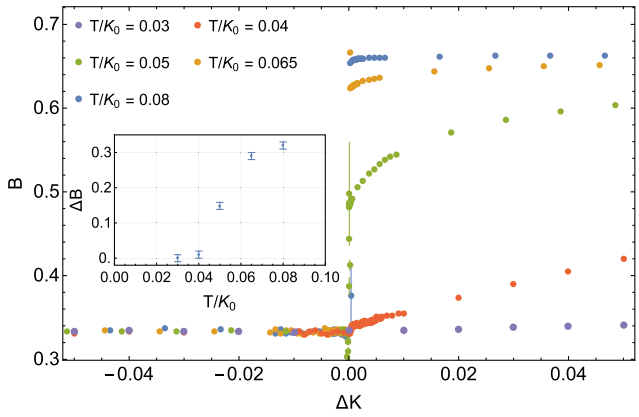

FIG. 12. Binder cumulant for several values of T/K_0 calculated at the highest value of N_S considered for each temperature. The discontinuity decreases with decreasing temperature, indicating that the transition becomes weakly first order.

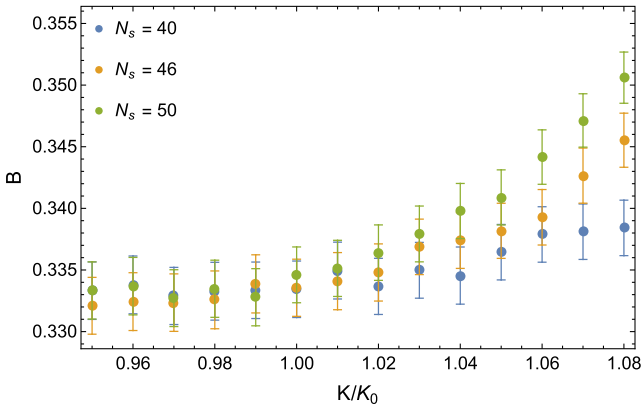

FIG. 13. Binder cumulant at $T/K_0 = 0.03$ for different spatial sizes. No discontinuity is observed at the phase transition, which is consistent with a second-order transition.

The collapse of the Binder cumulant data strongly depends on the value of $(K/K_0)_{\text{crit}}$ found. With the data shown in Fig. 13, it is difficult to specify precisely the point at which the curves for different spatial system sizes cross, and values of $(K/K_0)_{\text{crit}} \in [0.96, 1]$ are compatible with the data obtained. Motivated by the values of $(K/K_0)_{\text{crit}}$ obtained for higher temperatures, we take $(K/K_0)_{\text{crit}} = 0.97$ for $T/K_0 = 0.03$, and explore the values of the critical exponent ν that allow for the data to be collapsed.

To illustrate this, let us suppose that the transition is in the XY universality class. In four dimensions, the XY model is at its upper critical dimension so, for this scenario, we would expect mean field exponents with logarithmic corrections. Figure 14 shows an instance of a collapse for mean field exponent $\nu = 1/2$. Similar such plots are obtained for ν in the range 0.3–0.7 illustrating that the Monte Carlo data are consistent with a continuous transition below a temperature of $T/K_0 = 0.05$ with ν in the range 0.3–0.7 that includes the mean field exponent.

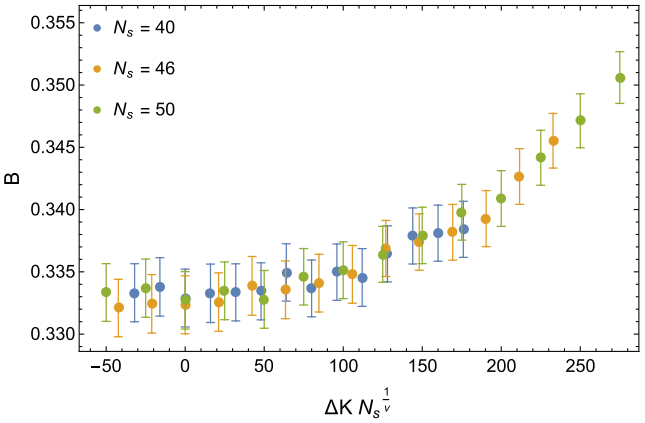

FIG. 14. Collapse of the Binder cumulant data at $T/K_0 = 0.03$ obtained for $\nu = 0.5$ and $(K/K_0)_{\text{crit}} = 0.97$.

IV. CONCLUSION

In this paper we have revisited the phase diagram of the $4D$ U(1) LGT using GPU accelerated Monte Carlo simulations on anisotropic lattices. Previous simulations had hinted at the presence of a tricritical point along the phase boundary separating the confined and deconfined phases.

We explored a range of lattice anisotropies with a rescaling of the couplings in the action to obtain phase diagram parametrized by the Hamiltonian couplings. This allows one to explore the phase diagram as a function of coupling β and temperature with considerable resolution in both couplings. We determined that there is a first-order region at $0.05 < T/K_0 \leq 0.175$, and a second-order region for $T/K_0 \geq 0.19$ with critical exponents consistent with those of the 3D XY universality class. These simulations clearly identify a tricritical point at intermediate temperatures between $T/K_0 = 0.175$ and $T/K_0 = 0.19$. For the region $T/K_0 \leq 0.05$ we find that the transition becomes more and more weakly first order as the temperature is lowered. Our simulations are compatible both with a continuous transition and a very weakly first-order transition in the zero temperature limit.

This paper reveals rich structure of the phase diagram in the pure gauge theory in four dimensions. If one switches on a coupling to scalar matter in the fundamental representation [3] the deconfined phase extends to finite matter coupling terminating in a tricritical point at the intersection of a first-order line, the Higgs transition and the confinement/deconfinement transition. It is of interest to explore the evolution of this phase diagram as a function of temperature in the light of the finite temperature tricriticality demonstrated in this work.

In this work we have chosen one approach to match parameters between the action and Hamiltonian formulations. To further confirm our findings it would be interesting, instead, to perform the calculation of the renormalized anisotropy through a matching of the helicity modulus [23,50] on both sides of the phase boundary.

ACKNOWLEDGMENTS

All authors thank Philippe de Forcrand for helpful comments on the manuscript and an enlightening discussion. R. T., N. C., P. B. and P. R. thank CeFEMA, an IST research unit whose activities are partially funded by FCT Contract No. UI/DB/04540/2020 for R&D Units. R. T. thanks CeFEMA for funding under FCT Contract No. UI/BD/154734/2023 and acknowledges computational resources provided under FCT Project No. 2023.10573.CPCA.A1.

APPENDIX A: DERIVATION OF THE ACTION

In this appendix we derive the action for the $U(1)$ lattice gauge theory, from the Hamiltonian, given by

$$H = \frac{U}{2}\sum_{r,\mu}(n_\mu(r))^2 - K\sum_{r,\mu<\nu}\cos\left[\Theta_{\mu\nu}(r)\right]. \tag{A1}$$

The Hilbert space is spanned by the states $|\phi\rangle = \otimes_{r,\mu}|\phi_\mu(r)\rangle$ or $|n\rangle = \otimes_{r,\mu}|n_\mu(r)\rangle$ such that $e^{i\hat{\phi}_\mu(r)}|\phi\rangle = e^{i\phi_\mu(r)}|\phi\rangle$ and $\hat{n}_\mu(r)|n\rangle = n_\mu(r)|n\rangle$.

As the operator $\hat{n}_\mu(r)$ corresponds to the lattice version of the electric field flux through the link $r+\hat{\mu}$, the counterpart of the Gauss law on the lattice is that the charge, q, on a lattice site r is given by the sum of the electric flux through the links connected to site r, given by the $\hat{n}_\mu(r)$ operators as

$$\hat{Q}_r = \sum_\mu[\hat{n}_\mu(r) + \hat{n}_\mu(r-\hat{\mu})] = q. \tag{A2}$$

We are interested in studying the U(1) LGT without charges, so we consider the projector to this subspace of the Hilbert space, written as

$$P = \prod_r \delta_{\hat{Q}_r,0} = \int\prod_r \frac{d\theta(r)}{2\pi}\, e^{i\sum_r \hat{Q}_r\theta(r)}, \tag{A3}$$

which has the properties $P^2 = P$ and $[P,H] = 0$. Thus, the partition function is given by $Z = \mathrm{tr}[e^{-\beta H}P]$.

In order to numerically simulate this theory, we perform a Trotter decomposition, by separating the partition function Z into N time intervals, with a temporal extent $\Delta\tau = \beta/N$, thus obtaining a partition function of the form $Z = \int D\phi D\theta \sum_n e^{-S[\phi,\theta,n]}$ with

$$\begin{aligned} S[\phi,\theta,n] = &-\Delta\tau K\sum_{\tau,r,\mu<\nu}\cos\left[\phi_\mu(\tau,r) - \phi_\nu(\tau,r+\hat{\mu}) + \phi_\mu(\tau,r+\hat{\nu}) - \phi_\nu(\tau,r)\right] \\ &- i\sum_{\tau,r,\mu}\left[\phi_\mu(\tau,r) - \phi_\mu(\tau+1,r) + \theta(\tau,r) + \theta(\tau,r+\hat{\mu})\right]n_\mu(\tau,r) + \Delta\tau\frac{U}{2}\sum_{\tau,r,\mu}\left[n_\mu(\tau,r)\right]^2. \end{aligned} \tag{A4}$$

In order to identify this action with a theory on a $(3+1)\mathcal{D}$ lattice, we identify $\hat{\theta}(\tau,r)$ with the phase of a link variable in the temporal direction, $\phi_0(\tau,r)$, so that the second term in Eq. (A4) corresponds to the phase of a space-time plaquette.

We can then approximate the sum over n in the partition function in Eq. (A4) for $\Delta\tau U \gg 1$ using the Villain approximation [51], given by

$$e^{z\cos(\Phi)} = \sum_n I_n(z)e^{in\Phi} \simeq \sum_n e^{-\frac{1}{2z}n^2 + i\Phi n}, \tag{A5}$$

which is valid for $z \gg 1$. Then, we obtain the approximated partition function, given by $Z = \int D\phi e^{-S[\phi]}$ with the action $S[\phi]$ given in Eq. (9), where we relabelled the spacetime coordinates as $n = (\tau, r)$ with directions $\mu,\nu = (0,1,2,3)$ with $\mu = 0$ for the temporal direction.

APPENDIX B

In this appendix, we describe a systematic perturbative approach to matching the parameters in the action and Hamiltonian formulations of the lattice gauge theory.

A naive matching of the coefficients multiplying the spatial and space-time parts of the action in Eq. (2) and Hamiltonian (6) is as follows. We first note that the interval $\Delta\tau$ used in the Trotter decomposition coincides with the lattice spacing in the temporal direction. Then we may write the temperature as $T = \frac{1}{N_t\Delta\tau}$ and find the following relations between the simulation parameters and the Hamiltonian parameters

$$\frac{K}{U} = \beta^2, \qquad \frac{T}{U} = \frac{\beta\xi}{N_t}. \tag{B1}$$

We determine the critical value of the coupling, β_c, for different values of N_t and for each value of the anisotropy parameter. Figure 15 shows these points parametrized using the relations in Eq. (B1).

Evidently the points for different ξ in Fig. 15 do not collapse to a single phase transition line. This is a consequence of effectively parametrizing the Hamiltonian from the action at weak coupling (large β). In particular, as discussed in Appendix A, where we derived the action in Eq. (A4) from the Hamiltonian, we took $z = \frac{1}{\Delta\tau U}$. However,

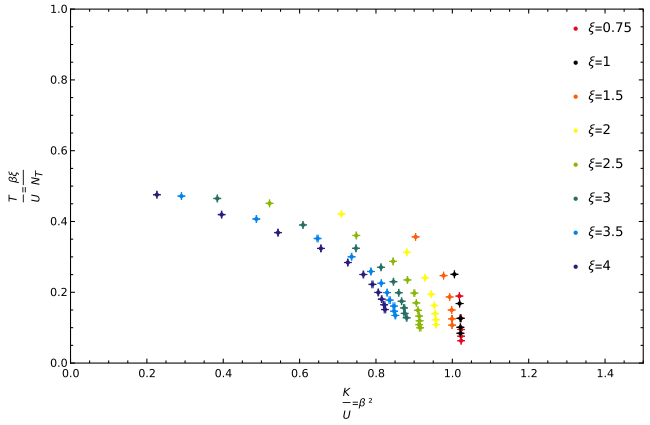

FIG. 15. Position of the peaks in the Polyakov loop susceptibility in terms of the quantities in Eq. (B1).

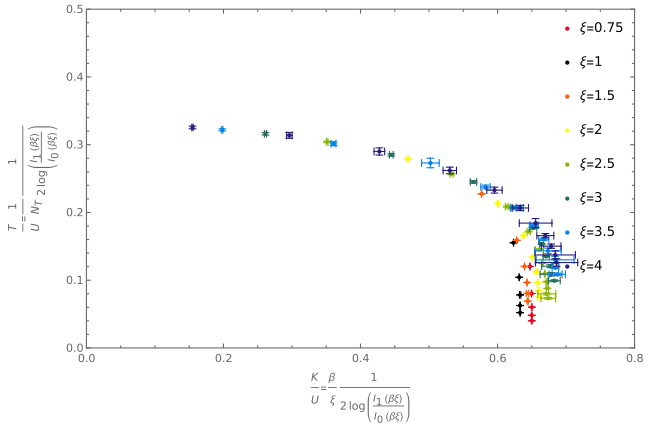

FIG. 16. Phase diagram using the relations in Eq. (B4).

this approximation is valid only in the limit of large z [48]. One may systematically improve the correspondence between the two formulations by revisiting the Villain approximation [Eq. (A5)] used to derive one from the other.

So instead we take

$$e^{z\cos(\Phi)} = \sum_n I_n(z) e^{in\Phi} \simeq \sum_n e^{-\frac{1}{2z_V}n^2 + i\Phi n}, \tag{B2}$$

with $z_V = -\frac{1}{2\log(\frac{I_1(z)}{I_0(z)})}$. In the limit $z \to \infty$, we have $z_V \approx z$ and we recover Eq. (A5). Using now the approximation in Eq. (B2) in the action in Eq. (A4) with $z_V = \frac{1}{\Delta\tau U}$ we obtain

$$\begin{aligned} S[\phi] = &-\Delta\tau K \sum_{n,\mu<\nu} \cos\left[\phi_\mu(n) + \phi_\nu(n+\hat{\mu}) - \phi_\mu(n+\hat{\nu}) - \phi_\nu(n)\right] \\ &- z\sum_{n,\mu} \cos\left[\phi_\mu(n) + \phi_0(n+\hat{\mu}) - \phi_\mu(n+e_0) - \phi_0(n)\right], \end{aligned} \tag{B3}$$

with z such that $\frac{1}{\Delta\tau U} = -\frac{1}{2\log(\frac{I_1(z)}{I_0(z)})}$. We match the coefficients multiplying the spatial and space-time parts of the action in Eq. (B3) with the ones in the simulated action, in Eq. (2). This leads to

$$\frac{K}{U} = -\frac{\beta}{\xi}\frac{1}{2\log\left(\frac{I_1(\beta\xi)}{I_0(\beta\xi)}\right)}, \qquad \frac{T}{U} = -\frac{1}{N_t}\frac{1}{2\log\left(\frac{I_1(\beta\xi)}{I_0(\beta\xi)}\right)}. \tag{B4}$$

We can now plot the critical points at which the phase transition occurs for each value of N_t and ξ in terms of the quantities defined in Eq. (B4) and obtain the phase diagram shown in Fig. 16.

With this approach, the points for different ξ collapse reasonably well over much of the phase transition line with notable lack of collapse only for large $\frac{K}{U}$. Having understood how to improve the matching conditions directly from the Villain approximation, in the main text we write a general Ansatz for the action that achieves a perfect collapse over the entire phase transition line.

APPENDIX C

TABLE I. Values of the phase diagram parameters $\frac{T}{K_0}$ and $\frac{K}{K_0}$, calculated for each value of ξ and N_t, used in the plot of the phase diagram in Fig. 4.

ξ	N_t	N_s	$\frac{K}{K_0}$	$\frac{T}{K_0}$
0.75	4	24	0.9956 ± 0.0001	0.18498 ± 0.00001
0.75	6	24	0.9996 ± 0.0001	0.12356 ± 0.00001
0.75	8	24	1.0002 ± 0.0002	0.09270 ± 0.00001
0.75	10	24	1.0000 ± 0.0002	0.07415 ± 0.00001
0.75	12	24	1.0001 ± 0.0003	0.01797 ± 0.00001
1	4	24	0.9844 ± 0.0001	0.2454 ± 0.00001
1	6	24	0.9978 ± 0.0001	0.16473 ± 0.00001
1	8	24	0.9999 ± 0.00012	0.1237 ± 0.0001
1	10	24	0.9999 ± 0.0005	0.09895 ± 0.00004
1	12	24	1.0000 ± 0.0001	0.08245 ± 0.00001
1.5	4	24	0.9009 ± 0.0001	0.3554 ± 0.0001

(Table continued)

TABLE I. *(Continued)*

ξ	N_t	N_s	$\frac{K}{K_0}$	$\frac{T}{K_0}$
1.5	6	24	0.9776 ± 0.0001	0.24730 ± 0.00003
1.5	8	24	0.9944 ± 0.0001	0.18711 ± 0.00002
1.5	10	24	0.9999 ± 0.0002	0.15012 ± 0.00002
1.5	12	24	1.0009 ± 0.0015	0.12516 ± 0.00002
1.5	14	24	1.0014 ± 0.0005	0.1073 ± 0.0001
2	4	24	0.7209 ± 0.0005	0.4280 ± 0.0003
2	6	24	0.9107 ± 0.0005	0.3234 ± 0.0001
2	8	24	0.9646 ± 0.0005	0.2503 ± 0.0001
2	10	24	0.9831 ± 0.0001	0.2023 ± 0.00003
2	12	24	0.9923 ± 0.0006	0.1694 ± 0.0001
2	14	24	0.9947 ± 0.0003	0.14541 ± 0.00004
2	16	24	0.9966 ± 0.0003	0.12736 ± 0.00004
2	18	24	0.9975 ± 0.0010	0.1133 ± 0.0001
2.5	4	24	0.5353 ± 0.0006	0.4634 ± 0.0005
2.5	6	24	0.7961 ± 0.0010	0.3834 ± 0.0004
2.5	8	24	0.9113 ± 0.0008	0.3098 ± 0.0003
2.5	10	24	0.9570 ± 0.0009	0.2547 ± 0.0002
2.5	12	24	0.9790 ± 0.0024	0.2149 ± 0.0005
2.5	14	24	0.9854 ± 0.0003	0.1849 ± 0.0001
2.5	16	24	0.9905 ± 0.0002	0.16225 ± 0.00002
2.5	18	24	0.9945 ± 0.0004	0.1445 ± 0.0001
2.5	20	24	0.9958 ± 0.0007	0.1302 ± 0.0001
2.5	22	24	0.9946 ± 0.0005	0.1183 ± 0.0006
2.5	24	24	0.9978 ± 0.0040	0.1086 ± 0.004
3	4	24	0.3968 ± 0.0009	0.4800 ± 0.0009
3	6	24	0.6598 ± 0.0011	0.4227 ± 0.0006
3	8	24	0.8316 ± 0.0016	0.3607 ± 0.0007
3	10	24	0.9149 ± 0.0014	0.3044 ± 0.0005
3	12	24	0.9566 ± 0.0018	0.2600 ± 0.0005
3	14	24	0.9745 ± 0.0010	0.2252 ± 0.0002
3	16	24	0.9841 ± 0.0014	0.1981 ± 0.0003
3	18	24	0.9926 ± 0.0040	0.1770 ± 0.0007
3	20	24	0.9944 ± 0.0050	0.1594 ± 0.0008
3	22	24	1.0012 ± 0.0028	0.1455 ± 0.0004
3.5	4	24	0.3006 ± 0.0005	0.4880 ± 0.0007
3.5	6	24	0.5330 ± 0.0013	0.4457 ± 0.0010
3.5	8	24	0.7360 ± 0.0040	0.4003 ± 0.0022
3.5	10	24	0.8518 ± 0.0021	0.3475 ± 0.0008
3.5	12	24	0.9184 ± 0.0027	0.3020 ± 0.0009
3.5	14	24	0.9541 ± 0.0018	0.2644 ± 0.0005
3.5	16	24	0.9740 ± 0.0022	0.2340 ± 0.0005
3.5	18	24	0.9830 ± 0.0060	0.2091 ± 0.0012
3.5	20	24	0.9978 ± 0.0080	0.1897 ± 0.0015
3.5	22	24	0.9983 ± 0.0014	0.1725 ± 0.0002
3.5	24	24	1.0026 ± 0.0035	0.1585 ± 0.0005
4	4	24	0.2345 ± 0.0005	0.4929 ± 0.0010
4	6	24	0.4368 ± 0.0015	0.4629 ± 0.0015
4	8	24	0.6257 ± 0.0024	0.4244 ± 0.0016
4	10	24	0.7735 ± 0.0028	0.3821 ± 0.0014
4	12	24	0.8666 ± 0.0031	0.3389 ± 0.0012
4	14	24	0.9201 ± 0.0033	0.3002 ± 0.0010
4	16	24	0.9513 ± 0.0060	0.2674 ± 0.0018
4	18	24	0.9711 ± 0.0034	0.2404 ± 0.0008
4	20	24	0.9830 ± 0.0040	0.2178 ± 0.0008
4	22	24	0.9914 ± 0.0080	0.1989 ± 0.0016
4	24	24	0.9940 ± 0.0080	0.1826 ± 0.0015

(Table continued)

[1] K. G. Wilson, Phys. Rev. D **10**, 2445 (1974).
[2] T. Banks, R. Myerson, and J. Kogut, Nucl. Phys. **B129**, 493 (1977).
[3] E. Fradkin and L. Susskind, Phys. Rev. D **17**, 2637 (1978).
[4] G. Bhanot, Nucl. Phys. **B205**, 168 (1982).
[5] K. J. Moriarty, Phys. Rev. D **25**, 2185 (1982).
[6] J. S. Barber, Phys. Lett. **147B**, 330 (1984).
[7] S. D. Drell, H. R. Quinn, B. Svetitsky, and M. Weinstein, Phys. Rev. D **19**, 619 (1979).
[8] V. Azcoiti, G. Di Carlo, and A. Grillo, Phys. Lett. B **258**, 207 (1991).
[9] V. Azcoiti, G. Di Carlo, and A. Grillo, Phys. Lett. B **268**, 101 (1991).
[10] G. Arnold, B. Bunk, T. Lippert, and K. Schilling, Nucl. Phys. B, Proc. Suppl. **119**, 864 (2003).
[11] A. M. Polyakov, *Gauge Fields and Strings* (CRC Press, 1987), Vol. 3.
[12] A. M. Polyakov, Phys. Lett. **59B**, 82 (1975).
[13] A. H. Guth, Phys. Rev. D **21**, 2291 (1980).
[14] M. Creutz, L. Jacobs, and C. Rebbi, Phys. Rev. D **20**, 1915 (1979).
[15] B. Lautrup and M. Nauenberg, Phys. Lett. **95B**, 63 (1980).
[16] T. A. DeGrand and D. Toussaint, Phys. Rev. D **24**, 466 (1981).
[17] G. Bhanot, Phys. Rev. D **24**, 461 (1981).
[18] K. Mütter and K. Schilling, Nucl. Phys. **B200**, 362 (1982).
[19] J. Jersák, T. Neuhaus, and P. M. Zerwas, Phys. Lett. **133B**, 103 (1983).
[20] R. Gupta, M. A. Novotny, and R. Cordery, Phys. Lett. B **172**, 86 (1986).
[21] H. G. Evertz, T. Jersák, T. Neuhaus, and P. M. Zerwas, Nucl. Phys. **B251**, 279 (1985).
[22] M. Vettorazzo and P. de Forcrand, Nucl. Phys. **B686**, 85 (2004).
[23] M. Vettorazzo and P. de Forcrand, Phys. Lett. B **604**, 82 (2004).
[24] B. A. Berg and A. Bazavov, Proc. Sci. LAT2006 (**2006**) 061 [arXiv:0609006].

[25] C. Bonati and M. D'Elia, Phys. Rev. D **88**, 065025 (2013).
[26] J. S. Barber, R. E. Shrock, and R. Schrader, Phys. Lett. **152B**, 221 (1985).
[27] J. S. Barber and R. E. Shrock, Nucl. Phys. **B257**, 515 (1985).
[28] C. B. Lang and T. Neuhaus, Nucl. Phys. B, Proc. Suppl. **34**, 543 (1994).
[29] G. Arnold, K. Schilling, and T. Lippert, Phys. Rev. D **59**, 054509 (1999).
[30] J. Cox, T. Neuhaus, and H. Pfeiffer, Nucl. Phys. B, Proc. Suppl. **73**, 712 (1999).
[31] I. Campos, A. Cruz, and A. Tarancón, Phys. Lett. B **424**, 328 (1998).
[32] I. Campos, A. Cruz, and A. Tarancón, Nucl. Phys. **B528**, 325 (1998).
[33] B. Klaus and C. Roiesnel, Phys. Rev. D **58**, 114509 (1998).
[34] G. Arnold, B. Bunk, T. Lippert, and K. Schilling, Nucl. Phys. B, Proc. Suppl. **119**, 864 (2003).
[35] J. Cox, J. Jersak, H. Pfeiffer, T. Neuhaus, P. W. Stephenson, and A. Seyfried, Nucl. Phys. **B545**, 607 (1999).
[36] J. Engels, F. Karsch, H. Satz, and I. Montvay, Nucl. Phys. **B205**, 545 (1982).
[37] C. Gattringer and C. B. Lang, *Quantum Chromodynamics on the Lattice* (Springer, Berlin, 2010), Vol. 788.
[38] N. Metropolis, A. W. Rosenbluth, M. N. Rosenbluth, A. H. Teller, and E. Teller, J. Chem. Phys. **21**, 1087 (1953).
[39] W. K. Hastings, Biometrika **57**, 97 (1970).
[40] N. Cardoso and P. Bicudo, J. Comput. Phys. **230**, 3998 (2011).
[41] N. Cardoso and P. Bicudo, Comput. Phys. Commun. **184**, 509 (2013).
[42] A. Amado, N. Cardoso, M. Cardoso, and P. Bicudo, Acta Phys. Pol. B Proc. Suppl. **5**, 1129 (2012).
[43] P. Bicudo, N. Cardoso, and A. Sharifian, Phys. Rev. D **104**, 054512 (2021).
[44] M. Creutz, Phys. Rev. D **36**, 515 (1987).
[45] M. H. Quenouille, Biometrika **43**, 353 (1956).
[46] J. Tukey, Ann. Math. Stat. **29**, 614 (1958).
[47] J. Kogut and L. Susskind, Phys. Rev. D **11**, 395 (1975).
[48] W. Janke and H. Kleinert, Nucl. Phys. **B270**, 135 (1986).
[49] N. Cardoso and P. Bicudo, Phys. Rev. D **85**, 077501 (2012).
[50] P. de Forcrand, W. Unger, and H. Vairinhos, Phys. Rev. D **97**, 034512 (2018).
[51] J. Villain, J. Phys. (France) **36**, 581 (1975).